Nonlinear Effects Caused by Coupling Misalignment in Rotors Equipped with Journal Bearings

Paolo Pennacchi, Andrea Vania, Steven Chatterton
Dept. of Mechanical Engineering
Politecnico di Milano,
Via La Masa, 1, I-20156, Milano, Italy

1. ABSTRACT

Misalignment is one of the most common sources of trouble of rotating machinery when rigid couplings connect the shafts. Ideal alignment of the shafts is difficult to be obtained and rotors may present angular and/or parallel misalignment (defined also as radial misalignment or offset). During a complete shaft revolution, a periodical change of the bearings load occurs in hyperstatic shaft-lines, if coupling misalignment between the shafts is excessive. If the rotating machine is equipped with journal bearings, the change of the loads on the bearings causes also the variation of their instantaneous dynamic characteristics, i.e. damping and stiffness, and the complete system cannot be considered any longer as linear.

Despite misalignment is often observed in the practice, there are relatively few studies about this phenomenon in literature and their results are sometimes conflicting. The authors aim at modelling accurately this phenomenon, for the first time in this paper, and giving pertinent diagnostic information. The proposed method is suitable for every type of shaft-line supported by journal bearings. A finite element model is used for the hyperstatic shaft-line, while bearing characteristics are calculated by integrating Reynolds equation as a function of the instantaneous load acting on the bearings, caused also by the coupling misalignment. The results obtained by applying the proposed method are shown by means of the simulation, in the time domain, of the dynamical response of a hyperstatic shaft-line. Nonlinear effects are highlighted and the spectral components of the system response are analyzed, in order to give diagnostic information about the signature of this type of fault.

Keywords: *Coupling misalignment, hyperstatic rotors, journal bearings, rotordynamics, nonlinear effects.*

2. INTRODUCTION

In her comprehensive book about Rotordynamics, Muszyńska [1] observed that rotor misalignment could be considered as the second most common malfunction after unbalance. She remarked also that this interesting topic was not object of much attention by researchers.

The authors of this paper share her position and want to contribute by presenting a paper aimed at explaining the reason of the presence of superharmonic components, i.e. of nonlinear behaviour, in rotor vibration spectrum as a consequence of rigid coupling misalignment, owing to wrong assembly or imperfect flange machining, of an hyperstatic shaft-line equipped with journal bearings. The method is suitable to be applied to every type of shaft-line.

However, before dealing with this topic, it is necessary to observe, as it was also done by Lees [2], that the term “misalignment” is used to indicate several situations corresponding to different physical processes. Actually, various kinds of rotor misalignment were analyzed in literature.

A first group of papers considered the misalignment of the journal alone with respect to the bearing, without dealing with the complete dynamics of the shaft-line; some pioneering studies were presented by Boyd [3-4] and another example was given by Bou-Saïd and Nicolas [5]. A similar case was analyzed by Prabhu [6] that highlighted the effects of relative misalignment, between the journal and the bearing, on film thickness, friction and damping and found out superharmonics vibration response in the shaft. Bouyer and Fillon [7] observed experimentally that journal misalignment with respect to the bearing reduces hydrodynamic effects that could not counteract the relative misalignment, between the journal and the bearing, caused by an external applied torque.

Anyhow a shaft cannot be “simply” misaligned by itself: the causes of this type of malfunction are discussed by Bently [8], which also mentioned that misalignment produces additional loading on the bearings, but he did not present any mathematical model on the matter. On the contrary, several other papers considered both theoretical aspects and direct dynamic simulation of misalignment in Rotordynamics.

A group of papers considered misalignment between rotors joined by flexible couplings. Xu and Marangoni [9-10] studied the misalignment of a flexible coupling, highlighting the similarities with universal joint operation and the presence of 2X component in the vibration spectrum. In that study, the shaft-line was supported by ball bearings and the cause of the 2X component was ascribed to the variable stiffness of the flexible coupling as a consequence of the misalignment. Often papers in literature report that misalignment causes 2X components, but they neither consider the type of coupling nor the type of the bearings. Also Sekhar and Prabhu [11] considered flexible coupling, used Gibbons’ theoretical model [12] and performed some simulations in which 2X components were evident. Lee and Lee [13] used a test rig, equipped with ball bearings and flexible coupling, to verify the results of their theoretical model and observed the results on the orbit shape. Hu et al. [14] designed a test rig with flexible rotors equipped with three or more journal bearings suitable to study the misalignment. However, in this case, the focus is on “lateral misalignment” of the supports, rather than on coupling misalignment. Al-Hussain and Redmond [15] presented a theoretical model of two coupled Jeffcott rotors supported by rigid bearings. Radial misalignment was simulated and only 1X component resulted in the lateral vibration steady-state spectra. They observed also excitation of torsional vibrations. Al-Hussain proposed a further model about angular misalignment [16] affecting the flexible joint connecting two Jeffcott rotors installed on journal bearings. In this case only stability conditions were analyzed. A combination of theoretical analysis and experimental tests was presented by Patel and Darpe [17-18], which considered two identical Jeffcott rotors supported by ball bearings and connected by a pin-bush flexible coupling.

Another group of paper dealt with the diagnosis of misalignment using vibration measurements. Prabhakar et al. [19] presented a preliminary analysis about the use of continuous wavelet transform of the rotor vibration to detect flexible coupling misalignment. No experimental evidence was given as a support of the proposed method. Peng et al. [20-21] used improved wavelet analysis of vibration measurement in order to extract fault features in rotor system, including also coupling misalignment. Model based methods were also used: Sinha et al. [22] employed model parameter estimation of combined unbalance and misalignment of a couple of test rigs, performing sensitivity analysis as well. Saavedra and Ramírez [23-24] considered a test rig with a flexible coupling.

Pennacchi and Vania [25] used misalignment equivalent excitation in a model based approach to identify the misalignment of a flexible joint of a gas turbine unit.

The last group of papers considered the effects of rigid coupling misalignment: Bachschmid and Pennacchi [25] presented the successful identification of angular and radial misalignment in the shaft-line of a test-rig. Lees [2] focused his interest on rigid couplings, introducing a simple model that considers orientation and different tightening of the coupling bolts and neglects the presence of journal bearings. Nonlinear system response resulted as a consequence of coupling between torsional and lateral vibrations. Tsai and Huang [27] used a transfer matrix to model radial misalignment and found results similar to [15], even if they gave different motivations to the presence of 1X component only. More recently, Balahoo et al. [28] studied speed transients of a misaligned rotor with a rather simplified model. On the contrary, the model presented hereafter by the authors is suitable to study the behaviour of real rotating machinery, considering all the possible features.

It is evident, from the analysis of the current literature, that a complete analysis of the dynamic effect of rigid coupling misalignment on a real shaft-line, i.e. a hyperstatic shaft-line with several bearings and couplings like those used in turbo machines, is lacking. In this paper, the authors propose a complete and original method to simulate the behaviour of real shaft line, supported by several oil-film bearings, with rigid coupling misalignment. Nonlinear effects are highlighted and the spectral components of system response are analyzed, in order to give pertinent diagnostic information.

3. MODELLING OF RIGID COUPLING MISALIGNMENT IN REAL SHAFT-LINES

Usually, turbo machines are composed of some shafts connected by couplings, often of rigid type, and are supported by journal bearings. The resulting shaft-line is hyperstatic, like that represented in figure 1. The shaft-line, which represents a steam power unit, is composed of three different shafts, connected by two rigid couplings. In particular, the first shaft is the HP-IP (high pressure – intermediate pressure) turbine, the second is the LP (low pressure) turbine and the last one is the generator. However, the model proposed is applicable to other types of machines, with different number of couplings, shafts and bearings.

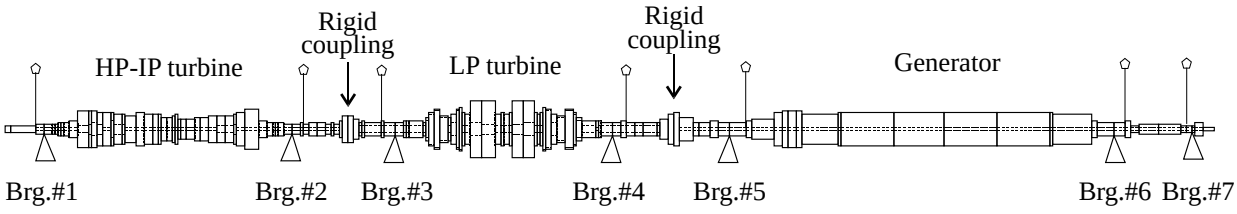

Figure 1. Example of hyperstatic shaft-line composed of three shafts. The vertical pennants indicate the position of vibration measuring planes.

The shaft-line is modelled in a standard way by means of a finite beam model and rigid disks, considering only the lateral vibrations, and 4 degrees of freedom (d.o.f.s) - two translational and two rotational - are considered per each node (see figure 2). Axial and torsional vibrations will be neglected. Considering the general j^{th} element of the shaft-line, the generalized displacement vector $\mathbf{x}_j^{(r)}$ of the j^{th} rotor node is ordered as follows:

$$\mathbf{x}_j^{(r)} = \left\{ x_j^{(r)} \quad \vartheta_{x_j}^{(r)} \quad y_j^{(r)} \quad \vartheta_{y_j}^{(r)} \right\}^{\mathrm{T}} \tag{1}$$

Two subsequent nodes, the j^{th} and the $(j+1)^{\text{th}}$, define the j^{th} element of the shaft-line. Index j is the main index used to order shaft nodes and elements. If the shaft-line has n_r nodes, thus $n_r - 1$ elements, the vector $\mathbf{x}^{(r)}$ of the generalized displacements of all the shaft-line nodes is composed by all the ordered vectors $\mathbf{x}_j^{(r)}$, as shown in eq. (2):

$$\mathbf{x}^{(r)} = \left\{ \mathbf{x}_1^{(r)\mathrm{T}} \quad \cdots \quad \mathbf{x}_{n_r}^{(r)\mathrm{T}} \right\}^{\mathrm{T}} = \left\{ x_1^{(r)} \quad \vartheta_{x_1}^{(r)} \quad y_1^{(r)} \quad \vartheta_{y_1}^{(r)} \cdots x_{n_r}^{(r)} \quad \vartheta_{x_{n_r}}^{(r)} \quad y_{n_r}^{(r)} \quad \vartheta_{y_{n_r}}^{(r)} \right\}^{\mathrm{T}} \tag{2}$$

The mass matrix of the rotor $[\mathbf{M}^{(r)}]$, which takes also into account the secondary effect of the rotatory inertia, the internal damping matrix $[\mathbf{C}^{(r)}]$, the stiffness matrix $[\mathbf{K}^{(r)}]$, which takes also into account the shear effect, and the gyroscopic matrix $[\mathbf{G}^{(r)}]$, all of order $(4n_r \times 4n_r)$, can be defined by means of standard Lagrange's methods, considering beam elements and rigid disks, as shown in [29-30]. Damping and gyroscopic matrices will be used in the following for the dynamic simulations.

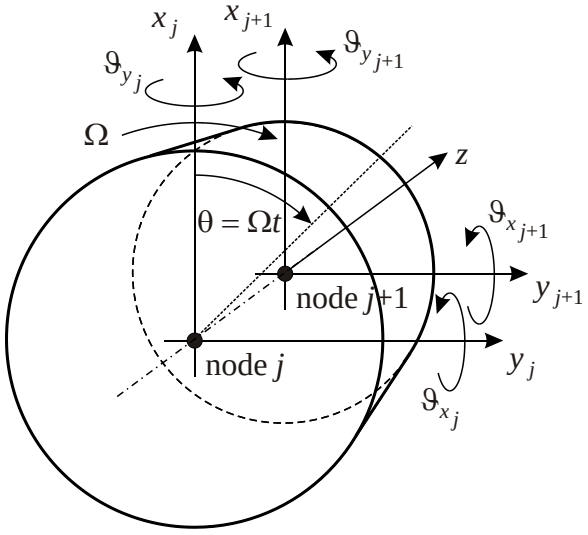

Figure 2. Degrees of freedom of the nodes of a general rotor element.

The shaft-line is supported on n_b journal bearings. They are located in correspondence of some nodes of the shaft, which are labelled by the indexes belonging to the set:

$$I_c = \left\{ j_{\text{Brg.\#1}} \quad \cdots \quad j_{\text{Brg.\#}n_b} \right\} \tag{3}$$

Shaft nodes whose indexes belong to I_c are defined as *constrained nodes* and the vector of their generalized displacements is indicated as $\mathbf{x}_c^{(r)}$, while the remaining nodes are the *free nodes* and the corresponding vector is $\mathbf{x}_f^{(r)}$:

$$\begin{aligned} \mathbf{x}_c^{(r)} &= \mathbf{x}_{j \in I_c}^{(r)} \\ \mathbf{x}_f^{(r)} &= \mathbf{x}_{j \notin I_c}^{(r)} \end{aligned} \tag{4}$$

During the machine installation, the shaft-line is statically aligned, using several methods like those described in [31], in order to nullify static bending moments and shear forces on the rigid coupling flanges. This is realized by displacing the supports in vertical directions with respect to the geodesic line, so that elements of $\mathbf{x}_c^{(r)}$ are generally not all null. The static centreline is a catenary.

If rigid couplings were also ideally aligned, without any radial or angular misalignment on their flanges, the static reaction forces on the bearings could be calculated, in order to determine the oil-film dynamic characteristics.

Otherwise, like described in this paper, it is necessary to take into account the effect of rigid coupling misalignment on the static centreline and, as a consequence, on the reaction forces of the bearing, considering that these forces are changing owing to the rotation of the shaft, i.e. to the orientation of the misalignment with respect to the phase reference.

3.1. Effect of rigid coupling misalignment on the shaft-line

Let's consider figure 3 in which a close up of a rigid coupling of the machine is shown. For the sake of simplicity, only a coupling is considered, being the model presented easily generalizable to n_C couplings.

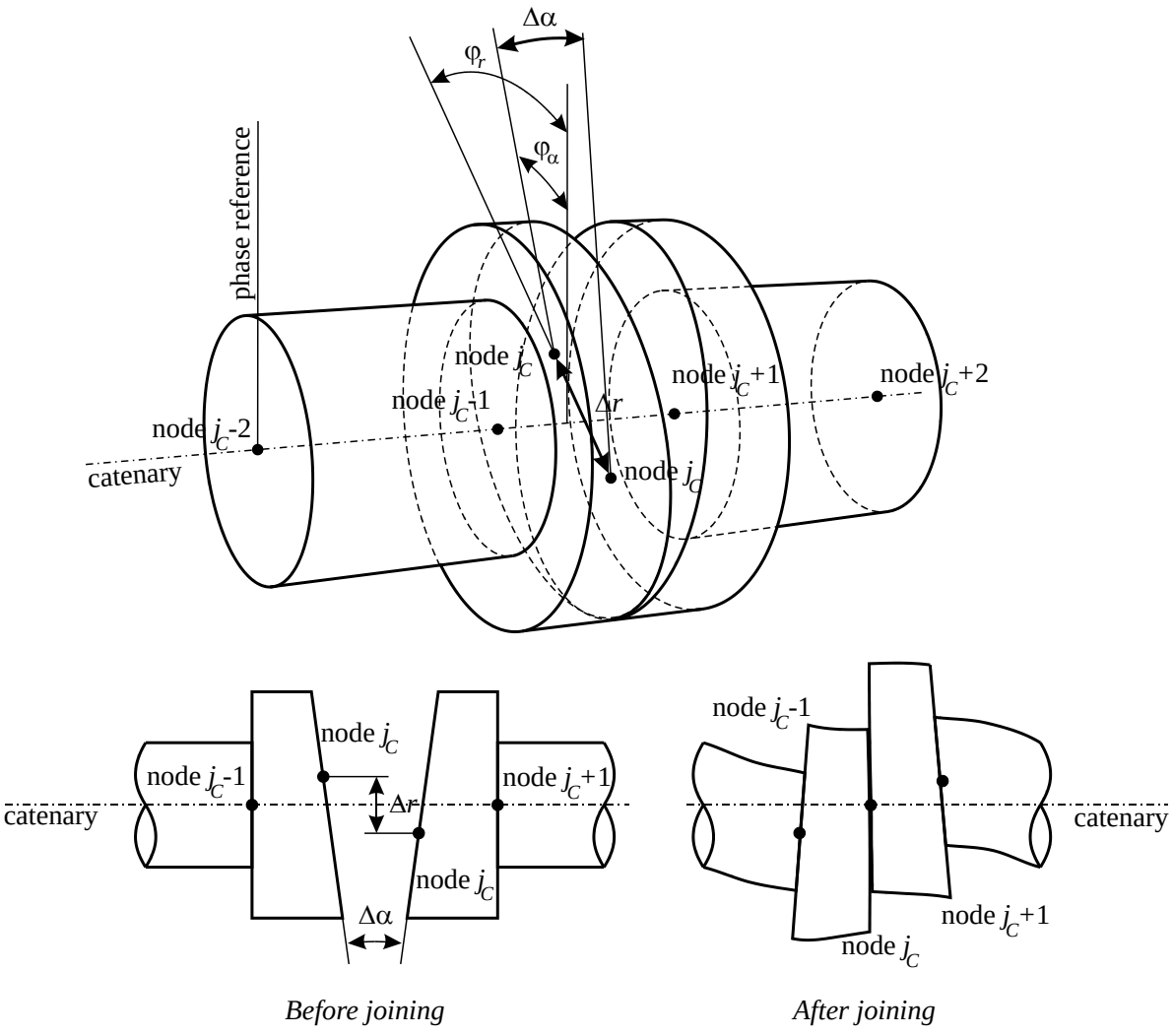

Figure 3. Rigid coupling misalignment: reference of angular and radial misalignment.

In the general case, the coupling faces are connected in correspondence of the $j_C{}^{\text{th}}$ shaft node and both radial and angular misalignment may occur as a consequence of a wrong mounting or imperfect machining. However, not only the magnitudes of these misalignments have to be considered, but also the relative phase with respect to the phase reference and the fact that the shaft is rotating with rotational speed Ω.

Hence, both types of misalignments are conveniently represented by means of rotating vectors, using for simplicity a complex notation [32]:

$$\begin{aligned} &\text{angular misalignment: } \Delta\alpha\, \mathrm{e}^{\mathrm{i}\varphi_\alpha}\, \mathrm{e}^{\mathrm{i}\Omega t}\, \varphi_\alpha \\ &\text{radial misalignment: } \quad \Delta r\, \mathrm{e}^{\mathrm{i}\varphi_r}\, \mathrm{e}^{\mathrm{i}\Omega t} \end{aligned} \tag{5}$$

Therefore, the effect of the rigid coupling misalignment is to impose generalized displacements $\Delta\mathbf{x}_j(\theta)$, which are function of the angular position $\theta = \Omega t$ of the shaft, on the d.o.f.s corresponding to the $j_C{}^{\text{th}}$ coupling node.

$$\Delta\mathbf{x}_{j_C}(\theta) = \begin{bmatrix} 1 & 0 \\ 0 & \mathrm{i} \\ \mathrm{i} & 0 \\ 0 & 1 \end{bmatrix} \begin{Bmatrix} \Delta r\, \mathrm{e}^{\mathrm{i}\varphi_r} \\ \Delta\alpha\, \mathrm{e}^{\mathrm{i}\varphi_\alpha} \end{Bmatrix} \mathrm{e}^{\mathrm{i}\Omega t} = \begin{bmatrix} 1 & 0 \\ 0 & \mathrm{i} \\ \mathrm{i} & 0 \\ 0 & 1 \end{bmatrix} \begin{Bmatrix} \Delta r\, \mathrm{e}^{\mathrm{i}\varphi_r} \\ \Delta\alpha\, \mathrm{e}^{\mathrm{i}\varphi_\alpha} \end{Bmatrix} \mathrm{e}^{\mathrm{i}\theta} \tag{6}$$

Vector $\Delta\mathbf{x}(\theta)$ representing all the displacements that are due to misalignment, has the same size of $\mathbf{x}^{(r)}$, i.e. $(4n_r \times 1)$, because the displacements of the d.o.f.s, which are not corresponding to the coupling nodes, are set equal to 0.

3.2. Calculation of the static reactions on the bearings

The static reactions $\mathbf{R}(\theta)$, i.e. the *load*, on the bearings can be calculated by imposing the static equilibrium of the free-body shaft-line and considering the imposed shaft alignment conditions, i.e. the displacements $\mathbf{x}_c^{(r)}$, that is:

$$\begin{aligned} \mathbf{R}(\theta) &= \left[\mathbf{K}^{(r)}\right]\left(\mathbf{x}^{(r)} + \Delta\mathbf{x}(\theta)\right) + \mathbf{W} = \\ &= \left[\mathbf{K}^{(r)}\right]\mathbf{x}^{(r)} + \left[\mathbf{K}^{(r)}\right]\Delta\mathbf{x}(\theta) + \mathbf{W} = \\ &= \left[\mathbf{K}^{(r)}\right]\mathbf{x}^{(r)} + \mathbf{F}_C(\theta) + \mathbf{W} \end{aligned} \tag{7}$$

where $\mathbf{W}$ is the weight force vector that can be calculated as:

$$\mathbf{W} = \left[\mathbf{M}^{(r)}\right]\left\{-g \quad 0 \quad 0 \quad 0 \quad \cdots \quad -g \quad 0 \quad 0 \quad 0\right\}^{\mathrm{T}} \tag{8}$$

and $\mathbf{F}_C(\theta)$ is the *equivalent force* due to the coupling misalignment. The only elements of vector $\mathbf{F}_C(\theta)$ that are different from zero are those corresponding to the d.o.f.s of $j_C{}^{\text{th}}$ node and they can be calculated by considering the stiffness submatrix corresponding to the $j_C{}^{\text{th}}$ node:

$$\mathbf{F}_C\big|_{j=j_C} = \left[\mathbf{K}^{(r)}\right]\Big\|_{j=j_C} \begin{bmatrix} 1 & 0 \\ 0 & \mathrm{i} \\ \mathrm{i} & 0 \\ 0 & 1 \end{bmatrix} \begin{Bmatrix} \Delta r\, \mathrm{e}^{\mathrm{i}\varphi_r} \\ \Delta\alpha\, \mathrm{e}^{\mathrm{i}\varphi_\alpha} \end{Bmatrix} \mathrm{e}^{\mathrm{i}\theta} \tag{9}$$

After these considerations, eq. (7) can be rewritten by reordering the d.o.f.s of the nodes and grouping the free and the constrained ones:

$$\begin{bmatrix} \mathbf{K}_{ff}^{(r)} & \mathbf{K}_{fc}^{(r)} \\ \mathbf{K}_{cf}^{(r)} & \mathbf{K}_{cc}^{(r)} \end{bmatrix} \begin{Bmatrix} \mathbf{x}_f^{(r)} \\ \mathbf{x}_c^{(r)} \end{Bmatrix} + \begin{Bmatrix} \mathbf{W}_f \\ \mathbf{W}_c \end{Bmatrix} + \begin{Bmatrix} \mathbf{F}_{C_f}(\theta) \\ \mathbf{0} \end{Bmatrix} = \begin{Bmatrix} \mathbf{0} \\ \mathbf{R}(\theta) \end{Bmatrix} \tag{10}$$

since, obviously, $\mathbf{F}_{C_c}(\theta) = \mathbf{0}$, because couplings are not in the same position of bearings.

The static free displacements as function of the angular position θ of the shaft are obtained as:

$$\mathbf{x}_f^{(r)}(\theta) = -\left[\mathbf{K}_{ff}^{(r)}\right]^{-1} \left(\left[\mathbf{K}_{fc}^{(r)}\right] \mathbf{x}_c^{(r)} + \mathbf{W}_f + \mathbf{F}_C(\theta) \right) \tag{11}$$

and the reactions on the bearings as:

$$\mathbf{R}(\theta) = \left[\mathbf{K}_{cf}^{(r)}\right] \mathbf{x}_f^{(r)} + \left[\mathbf{K}_{cc}^{(r)}\right] \mathbf{x}_c^{(r)} + \mathbf{W}_c \tag{12}$$

Notice that, due to the presence of the coupling misalignment, the reactions of eq. (12) have generally both the vertical and the horizontal components and that they are 1X periodical.

3.3. Calculation of the oil-film dynamic characteristics

It is commonly agreed that the static reactions on the bearings are used as the input loads to calculate the oil-film dynamic characteristics, because the static loads are largely predominant on the dynamical ones, due for instance to unbalances. However, the loads are not constant and depend on the angular position θ of the shaft, see eq. (12), in the case considered in the paper, as a consequence of the presence of the coupling misalignment. Hence, also the dynamic characteristics of the oil-film in the bearings have to be calculated as a function of θ. For the sake of simplicity, only constant rotational speeds will be taken into account. This notwithstanding, the proposed method could be easily extended also to speed transients.

Therefore, starting from the actual type and geometry of the n_b bearings, Reynolds equation in the isoviscous form [33-34] is used:

$$\frac{\partial}{\partial\xi}\left(\frac{h^3}{\eta}\frac{\partial p}{\partial\xi}\right) + \frac{\partial}{\partial\zeta}\left(\frac{h^3}{\eta}\frac{\partial p}{\partial\zeta}\right) = 6U\eta\frac{\partial h}{\partial\xi} + 12W \tag{13}$$

where ξ and ζ are the coordinates along the sliding and the axial directions respectively, η the viscosity, h the oil-film thickness, p the pressure, U the entraining velocity and W the relative velocity. Equation (13) is then expressed in non-dimensional form. The effects of small displacements and squeeze velocities are also introduced.

The integration of Reynolds equation is performed by using finite differences. The journal static equilibrium position is found by balancing the pressure distribution with the reactions $\mathbf{R}(\theta)$ in an iterative way. Then, the non-dimensional stiffness and damping coefficients are obtained for each static equilibrium position, using standard methods described in [33-34]. Also the corresponding

dimensional coefficients, $k_{rs_i}^{(b)}(\theta)$ and $c_{rs_i}^{(b)}(\theta)$, are calculated by means of those, considering the loads $\mathbf{R}(\theta)$.

4. SIMULATION OF SHAFT-LINE DYNAMICAL BEHAVIOUR

In order to perform the simulation of the dynamical behaviour of the shaft-line at the operating speed, a dynamical model has to be set-up. The matrices of the coupled shafts, i.e. the complete shaft-line, have been already introduced and now the effects owing to the foundation dynamics and to the oil-film characteristics are accounted for.

Different methods can be used to model the foundation. For the sake of brevity, only pedestals, i.e. lumped 2 d.o.f.s systems, will be considered. A discussion about other methods (modal or rigid) is reported in [35]. In a similar manner to the shaft-line, also the d.o.f.s of the foundation, represented by its horizontal and vertical displacements and connected by means of the n_b bearings to the rotor, can be ordered in a vector:

$$\mathbf{x}^{(f)} = \left\{ x_1^{(f)} \quad y_1^{(f)} \quad \cdots \quad x_{n_b}^{(f)} \quad y_{n_b}^{(f)} \right\}^{\mathrm{T}} \tag{14}$$

Therefore, the complete vector of the generalized displacements of the system is:

$$\mathbf{x} = \left\{ \mathbf{x}^{(r)\mathrm{T}} \quad \mathbf{x}^{(f)\mathrm{T}} \right\}^{\mathrm{T}} \tag{15}$$

The structure of $[\mathbf{M}^{(f)}]$, $[\mathbf{C}^{(f)}]$ and $[\mathbf{K}^{(f)}]$ is not relevant in this paper and depends on how the supporting structure is implemented, see [35].

The dynamic forces of the oil-film of the i^{th} bearing on the journal located at the j^{th} rotor node, as a consequence of dynamic displacements of the rotor d.o.f.s only, are:

$$\begin{aligned} \mathbf{F}_{b_i}^{(br)}(\theta) &= -\begin{bmatrix} k_{xx_i}^{(b)}(\theta) & 0 & k_{xy_i}^{(b)}(\theta) & 0 \\ 0 & 0 & 0 & 0 \\ k_{yx_i}^{(b)}(\theta) & 0 & k_{yy_i}^{(b)}(\theta) & 0 \\ 0 & 0 & 0 & 0 \end{bmatrix} \begin{Bmatrix} x_j^{(r)} \\ \vartheta_{x_j}^{(r)} \\ y_j^{(r)} \\ \vartheta_{y_j}^{(r)} \end{Bmatrix} - \begin{bmatrix} c_{xx_i}^{(b)}(\theta) & 0 & c_{xy_i}^{(b)}(\theta) & 0 \\ 0 & 0 & 0 & 0 \\ c_{yx_i}^{(b)}(\theta) & 0 & c_{yy_i}^{(b)}(\theta) & 0 \\ 0 & 0 & 0 & 0 \end{bmatrix} \begin{Bmatrix} \dot{x}_j^{(r)} \\ \dot{\vartheta}_{x_j}^{(r)} \\ \dot{y}_j^{(r)} \\ \dot{\vartheta}_{y_j}^{(r)} \end{Bmatrix} = \\ &= -\left[\mathbf{K}_i^{(b)}(\theta)\right]\mathbf{x}_j^{(r)} - \left[\mathbf{C}_i^{(b)}(\theta)\right]\dot{\mathbf{x}}_j^{(r)} \end{aligned} \tag{16}$$

while those that are due to the displacements of the supporting structure only, modelled by means of pedestals and corresponding to the i^{th} bearing, are:

$$\begin{aligned} \mathbf{F}_{b_i}^{(bf)}(\theta) &= -\begin{bmatrix} k_{xx_i}^{(b)}(\theta) & k_{xy_i}^{(b)}(\theta) \\ k_{yx_i}^{(b)}(\theta) & k_{yy_i}^{(b)}(\theta) \end{bmatrix} \begin{Bmatrix} x_j^{(f)} \\ y_j^{(f)} \end{Bmatrix} - \begin{bmatrix} c_{xx_i}^{(b)}(\theta) & c_{xy_i}^{(b)}(\theta) \\ c_{yx_i}^{(b)}(\theta) & c_{yy_i}^{(b)}(\theta) \end{bmatrix} \begin{Bmatrix} \dot{x}_j^{(f)} \\ \dot{y}_j^{(f)} \end{Bmatrix} = \\ &= -\left[\widehat{\mathbf{K}}_i^{(b)}(\theta)\right]\mathbf{x}_j^{(f)} - \left[\widehat{\mathbf{C}}_i^{(b)}(\theta)\right]\dot{\mathbf{x}}_j^{(f)} \end{aligned} \tag{17}$$

The actual bearing force between the rotor and the foundation is given by the difference between eq. (16) and eq. (17). In this way, the coupling effect of the oil-film forces is taken into account by the relative displacements of the nodes of the rotor and of the foundation in correspondence of the bearings. Thus, the fully assembled system of equation is built up.

This requires the definition of the stiffness coupling matrices $[\mathbf{K}^{(rr)}]$, $[\mathbf{K}^{(rf)}]$, $[\mathbf{K}^{(fr)}]$, $[\mathbf{K}^{(ff)}]$ and the corresponding damping matrices $[\mathbf{C}^{(rr)}]$, $[\mathbf{C}^{(rf)}]$, $[\mathbf{C}^{(fr)}]$, $[\mathbf{C}^{(ff)}]$, which are sparse and of order $(4n_r \times 4n_r)$, $(4n_r \times 2n_b)$, $(2n_b \times 4n_r)$ and $(2n_b \times 2n_b)$ respectively. The structure for the stiffness matrices is:

$$[\mathbf{K}^{(rr)}(\theta)] = \mathrm{diag}\left(\cdots \quad \left[\mathbf{K}_i^{(b)}(\theta)\right] \quad \cdots\right) \tag{18}$$

$$[\mathbf{K}^{(fr)}(\theta)] = \begin{bmatrix} \cdots & \cdots & \cdots & \cdots & \cdots & \cdots \\ \cdots & k_{xx_i}^{(b)}(\theta) & 0 & k_{xy_i}^{(b)}(\theta) & 0 & \cdots \\ \cdots & k_{yx_i}^{(b)}(\theta) & 0 & k_{yy_i}^{(b)}(\theta) & 0 & \cdots \\ \cdots & \cdots & \cdots & \cdots & \cdots & \cdots \end{bmatrix} \tag{19}$$

$$[\mathbf{K}^{(rf)}(\theta)] = \begin{bmatrix} \cdots & \cdots & \cdots & \cdots \\ \cdots & k_{xx_i}^{(b)}(\theta) & k_{xy_i}^{(b)}(\theta) & \cdots \\ \cdots & 0 & 0 & \cdots \\ \cdots & k_{yx_i}^{(b)}(\theta) & k_{yy_i}^{(b)}(\theta) & \cdots \\ \cdots & 0 & 0 & \cdots \\ \cdots & \cdots & \cdots & \cdots \end{bmatrix} \tag{20}$$

$$[\mathbf{K}^{(ff)}(\theta)] = \mathrm{diag}\left(\cdots \quad \left[\widehat{\mathbf{K}}_i^{(b)}(\theta)\right] \quad \cdots\right) \tag{21}$$

Damping coupling matrices have similar structure. The fully assembled system of equations, without external excitation, results:

$$\left[\mathbf{M}\right]\ddot{\mathbf{x}} + \left[\mathbf{C}(\theta)\right]\dot{\mathbf{x}} + \left[\mathbf{K}(\theta)\right]\left(\mathbf{x} + \Delta\mathbf{x}(\theta)\right) = \mathbf{0} \tag{22}$$

with:

$$[\mathbf{M}] = \begin{bmatrix} [\mathbf{M}^{(r)}] & \mathbf{0} \\ \mathbf{0} & [\mathbf{M}^{(f)}] \end{bmatrix} \tag{23}$$

$$[\mathbf{C}(\theta)] = \begin{bmatrix} [\mathbf{C}^{(r)}] + \Omega[\mathbf{G}^{(r)}] + [\mathbf{C}^{(rr)}(\theta)] & -[\mathbf{C}^{(rf)}(\theta)] \\ -[\mathbf{C}^{(fr)}(\theta)] & [\mathbf{C}^{(f)}] + [\mathbf{C}^{(ff)}(\theta)] \end{bmatrix} \tag{24}$$

$$[\mathbf{K}(\theta)] = \begin{bmatrix} [\mathbf{K}^{(r)}] + [\mathbf{K}^{(rr)}(\theta)] & -[\mathbf{K}^{(rf)}(\theta)] \\ -[\mathbf{K}^{(fr)}(\theta)] & [\mathbf{K}^{(f)}] + [\mathbf{K}^{(ff)}(\theta)] \end{bmatrix} \tag{25}$$

The remaining external forcing systems acting on the shaft-line are the weight $\mathbf{W}$ and the residual unavoidable unbalance distribution, which will be taken into account by the *equivalent unbalance* at the j_u[th] node:

$$\begin{aligned} \mathbf{F}_u(t) &= \begin{bmatrix} 0 & \vdots & 1 & 0 & \mathrm{i} & 0 & \vdots & 0 \end{bmatrix}^{\mathrm{T}} m_u r_u \Omega^2 \, \mathrm{e}^{\mathrm{i}\varphi_u} \, \mathrm{e}^{\mathrm{i}\Omega t} = \\ &= \begin{bmatrix} 0 & \vdots & 1 & 0 & \mathrm{i} & 0 & \vdots & 0 \end{bmatrix}^{\mathrm{T}} m_u r_u \Omega^2 \, \mathrm{e}^{\mathrm{i}\varphi_u} \, \mathrm{e}^{\mathrm{i}\theta} = \mathbf{F}_u(\theta) \end{aligned} \tag{26}$$

By considering all the external forcing and eq. (7), the fully assembled system of equations is nonlinear, because many of its terms depend on the angular position $\theta = \Omega t$:

$$\left[\mathbf{M}\right]\ddot{\mathbf{x}} + \left[\mathbf{C}(\theta)\right]\dot{\mathbf{x}} + \left[\mathbf{K}(\theta)\right]\mathbf{x} = -\bar{\mathbf{F}}_C(\theta) - \bar{\mathbf{W}} + \bar{\mathbf{F}}_u(\theta) \tag{27}$$

where the over-bars indicate that the corresponding vectors are padded with zeros in positions corresponding to foundation d.o.f.s.

The nonlinear system of equations in (27) is integrated in the time domain using the Newmark's implicit method, in which all the quantities depending on θ are evaluated for each integration step.

4.1. Simulation results

The machine, the model of which has been used for the simulations with the described method, is a steam turbo-generator unit of about 320 MVA, already sketched in figure 1 and described in detail in [36]. Node number is 175 and bearings #1, #2 and #7 are of tilting pad type, while the others of 2-lobes type.

Figure 4 shows the static reaction calculated in case of ideal alignment of the shaft-line, i.e. when the centreline follows a catenary and $\Delta\mathbf{x}(\theta) = \mathbf{0}$. Obviously, static reactions have only the vertical component, while the reaction on bearing #7 is very small and can be barely seen in the figure.

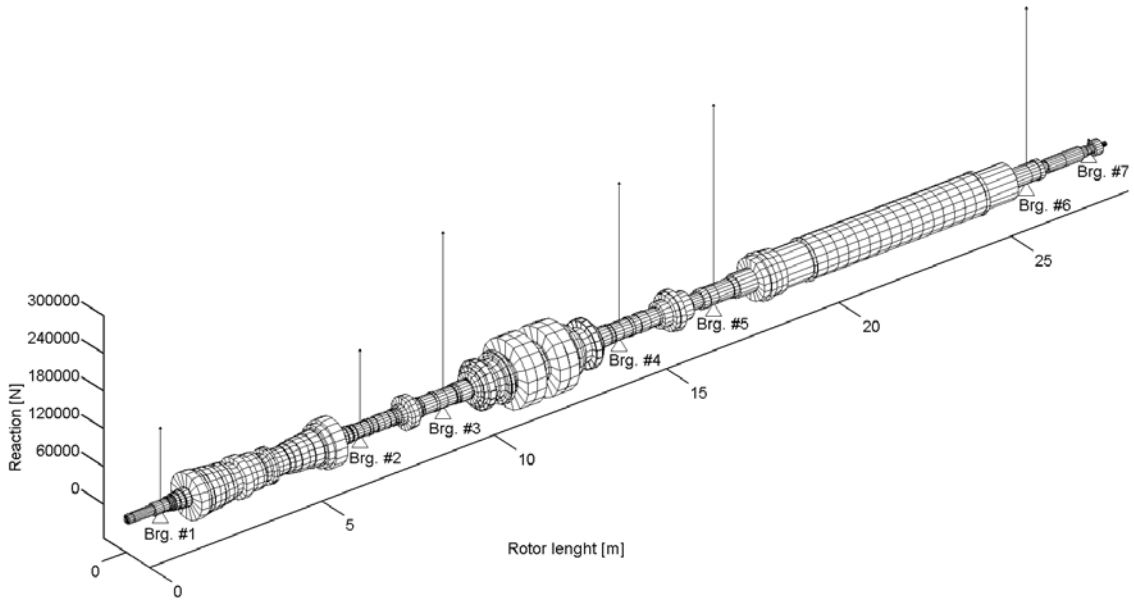

Figure 4. Static reactions in case of ideal alignment of the rigid couplings.

Different combinations of radial and angular misalignment conditions of the rigid coupling between HP-IP and LP turbines have been analysed. The first step of the proposed method is the calculation of the loads $\mathbf{R}(\theta)$: figure 5 and figure 6 illustrate the effect of radial and angular misalignment for two cases. The vectors of the static reactions are plotted vs. the angular rotation over a complete revolution. It is easy to observe that static reactions do not have only vertical component and that loads $\mathbf{R}(\theta)$ change remarkably on the bearings closer to the misaligned rigid

coupling, i.e. bearings #2 and #3. Some effects can be appreciated also on bearings #1 and #4, while practically there are not changes on generator bearings. Since in the following, without loss of generality, only the misalignment of the rigid coupling between HP-IP and LP turbines will be considered, whereas the dynamical response on generator bearings will not be considered.

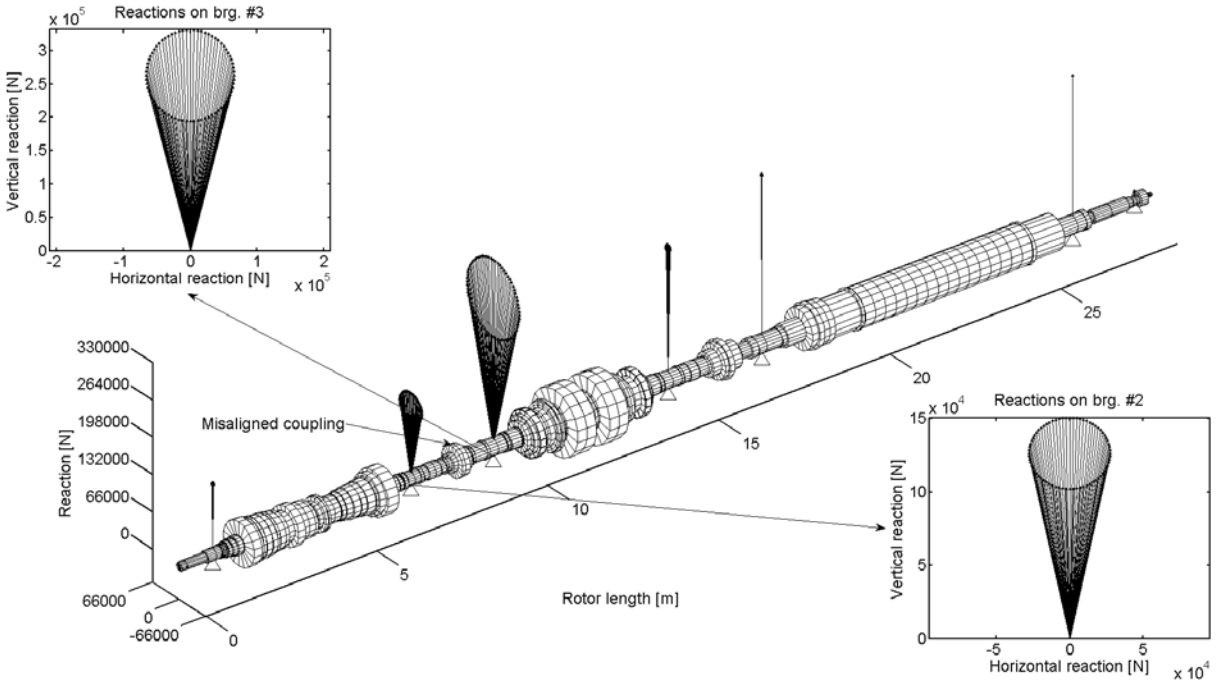

Figure 5. Static reactions in case of radial misalignment of 50 μm @ 0° of the coupling between HP-IP and LP turbine.

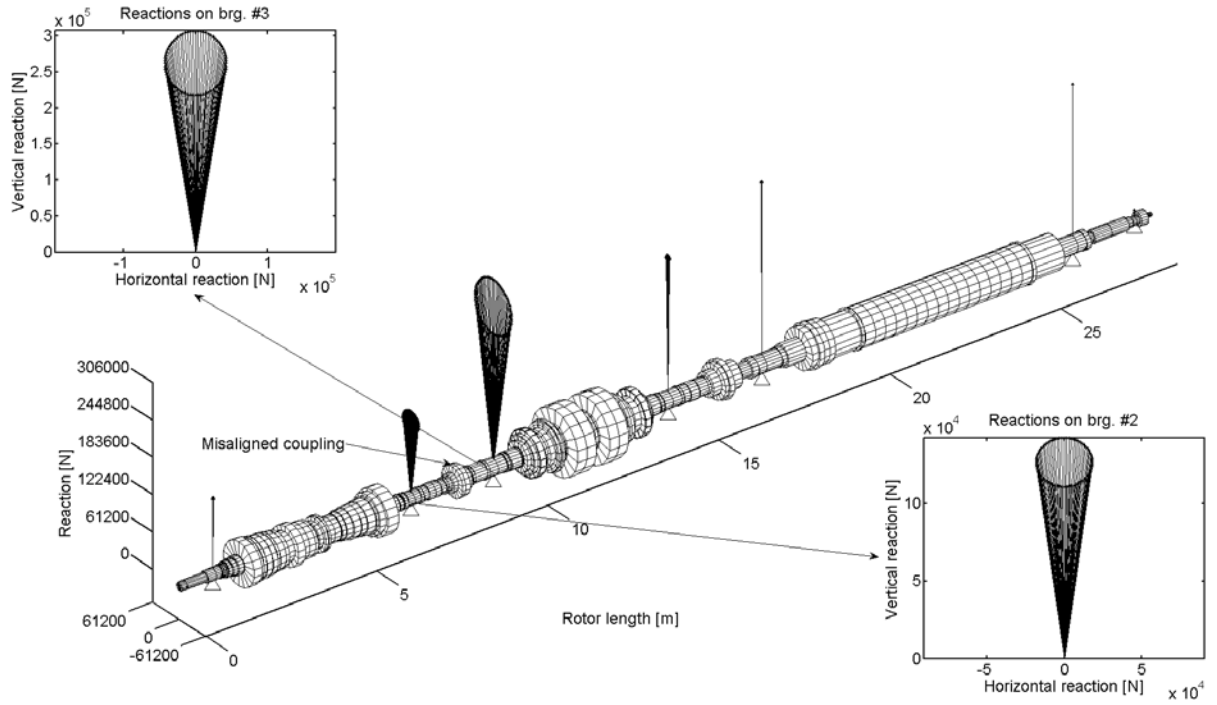

Figure 6. Static reactions in case of angular misalignment of 5 mrad @ 0° of the coupling between HP-IP and LP turbine.

The simulation of the dynamic response of the shaft-line is performed at the operating speed of 3000 rpm, considering also the presence of an unbalance placed about in the middle of the LP turbine (0.3 kgm with phase 0°).

An example is shown in figure 7, where only the steady-state shaft orbits in the vibration measuring plane close to bearings from #1 to #4 are shown. These measuring planes are actually external to the journal bearings, and their exact positions along the shaft line are indicated by the "pentagonal pennants" in figure 1. In this case, radial misalignment of 100 μm @ 90° and angular misalignment of 15 mrad @ 0° have been applied. Orbits in generator bearings are less affected by the misalignment and are not shown for the same reasons explained before. Similarly, the orbits in the other nodes of the shaft-line are not displayed both for the sake of brevity and because they are never measured in the practice.

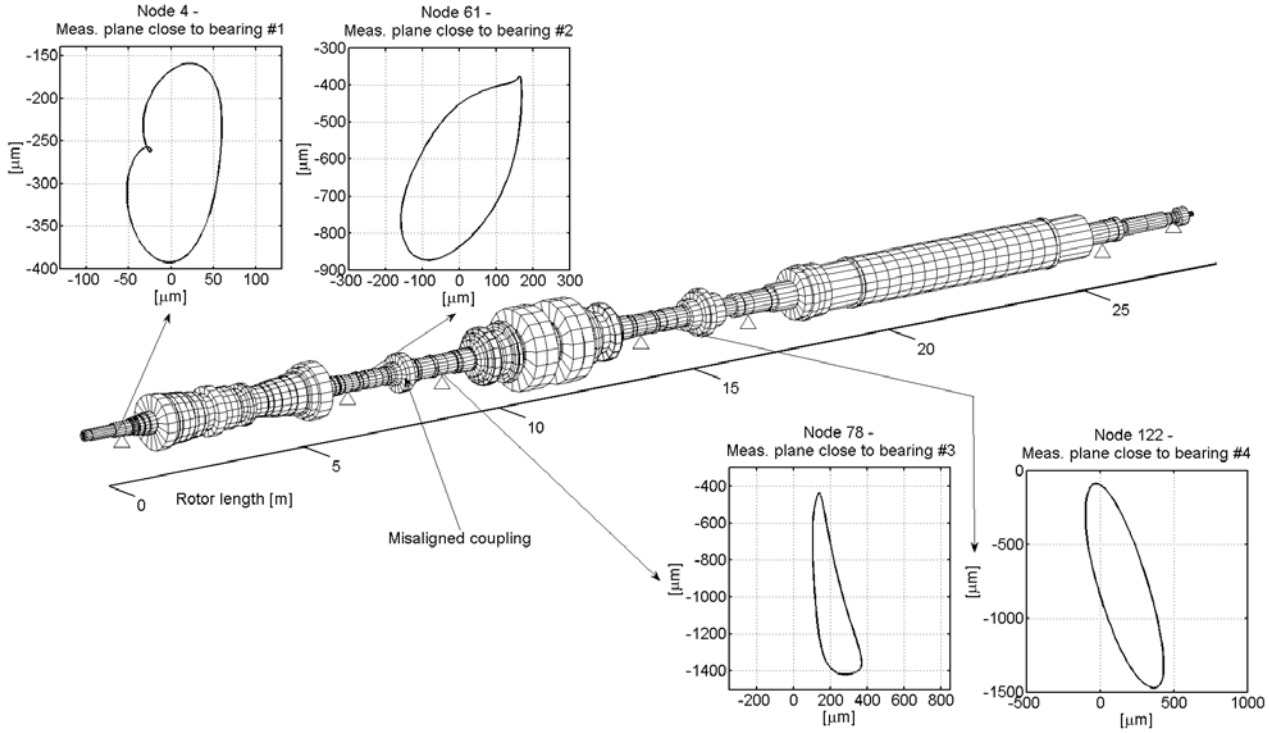

Figure 7. Shaft-line orbits in bearings from #1 to #4 in case of radial misalignment of 100 μm @ 90° and angular misalignment of 15 mrad @ 0°.

The case considered would be already critical in the reality and these vibration amplitudes would be dangerous for the actual rotating machine, because the bearing clearance would be exceeded. Orbits, in the measuring planes close to bearings from #1 to #3, show rather clearly the presence of superharmonics components (owing to the deformed shape with respect to the elliptical one) and the presence of nonlinear effects. These considerations are clearer from figure 8 to figure 11, where the full spectra of the vibration, corresponding to the orbits in the measuring planes close to bearings from #1 to #4, are considered.

Even though a logarithmic scale is used for the amplitudes, it is easy to observe that at least ±2X and ±3X components have remarkable amplitudes (i.e. measurable, the horizontal dashed lines in the figures indicate the amplitude of 1 μm) in the bearings from #1 to #3. Bearing #4 is rather "far" from the misaligned coupling and does not "feel" so much the effect of the misalignment: higher harmonic components are much smaller than the ±1X component.

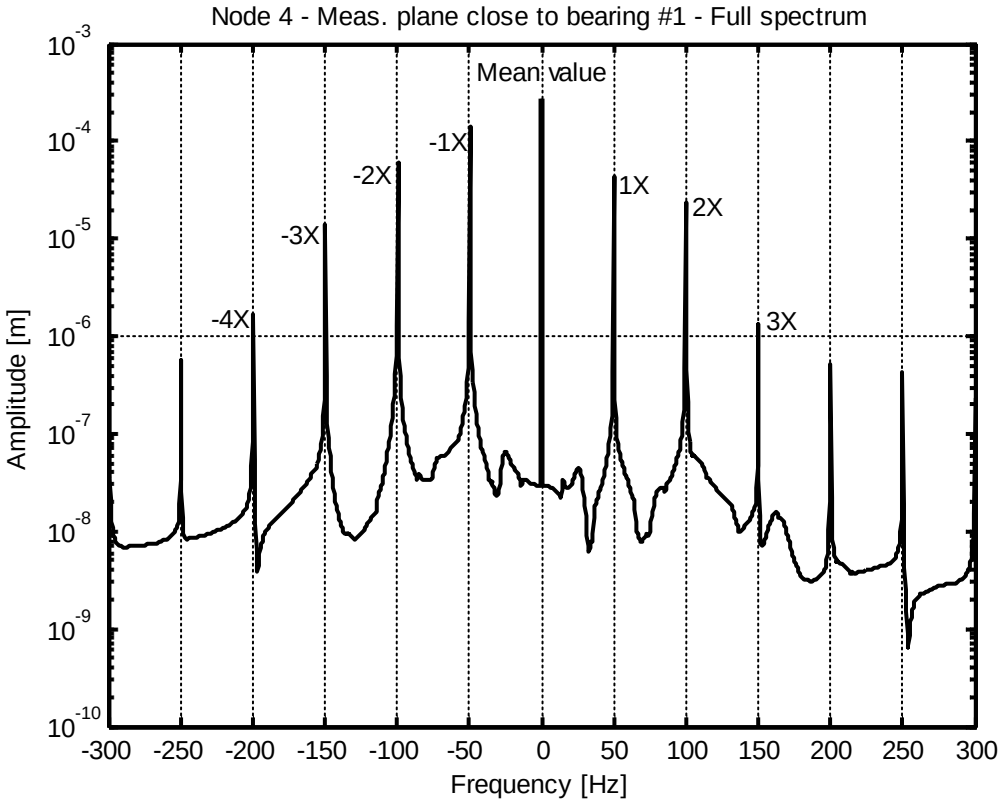

Figure 8. Full spectrum of shaft-line orbit close to bearing #1 in case of radial misalignment of 100 μm @ 90° and angular misalignment of 15 mrad @ 0°.

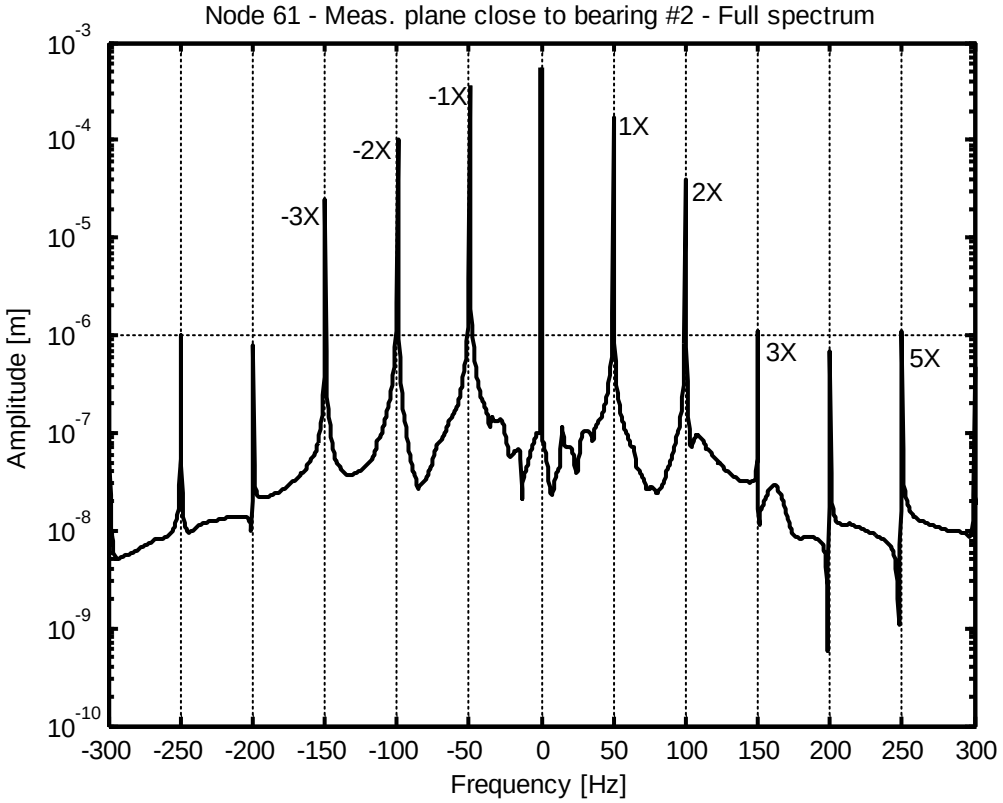

Figure 9. Full spectrum of shaft-line orbit close to bearing #2 in case of radial misalignment of 100 μm @ 90° and angular misalignment of 15 mrad @ 0°.

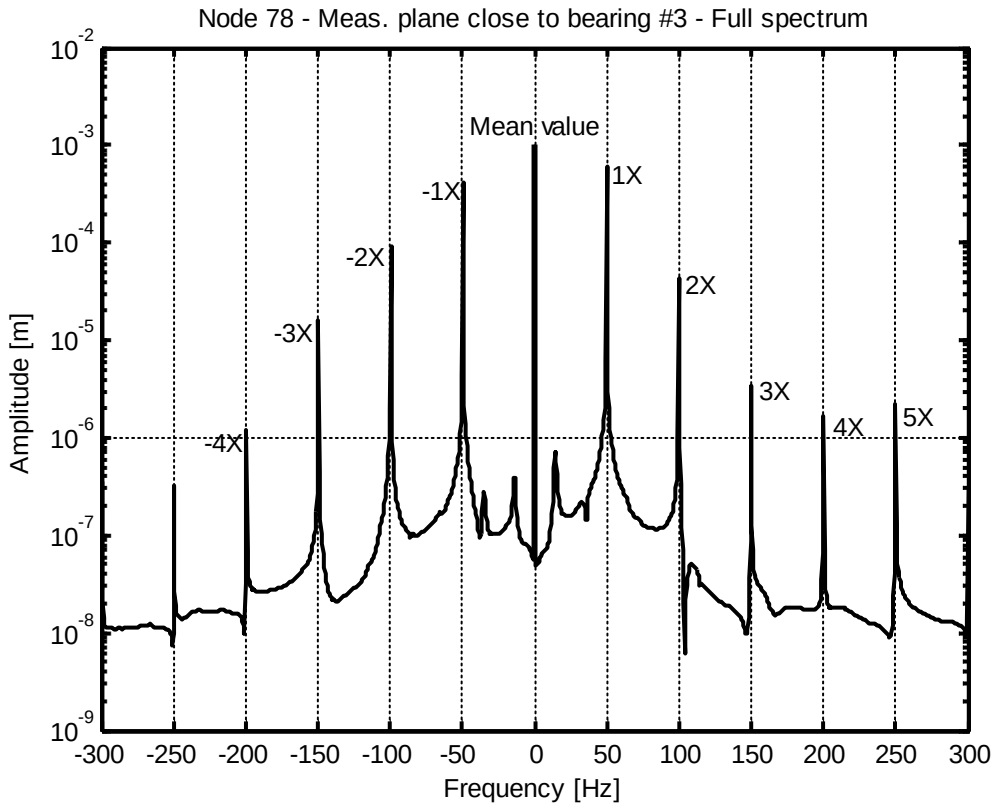

Figure 10. Full spectrum of shaft-line orbit close to bearing #3 in case of radial misalignment of 100 μm @ 90° and angular misalignment of 15 mrad @ 0°.

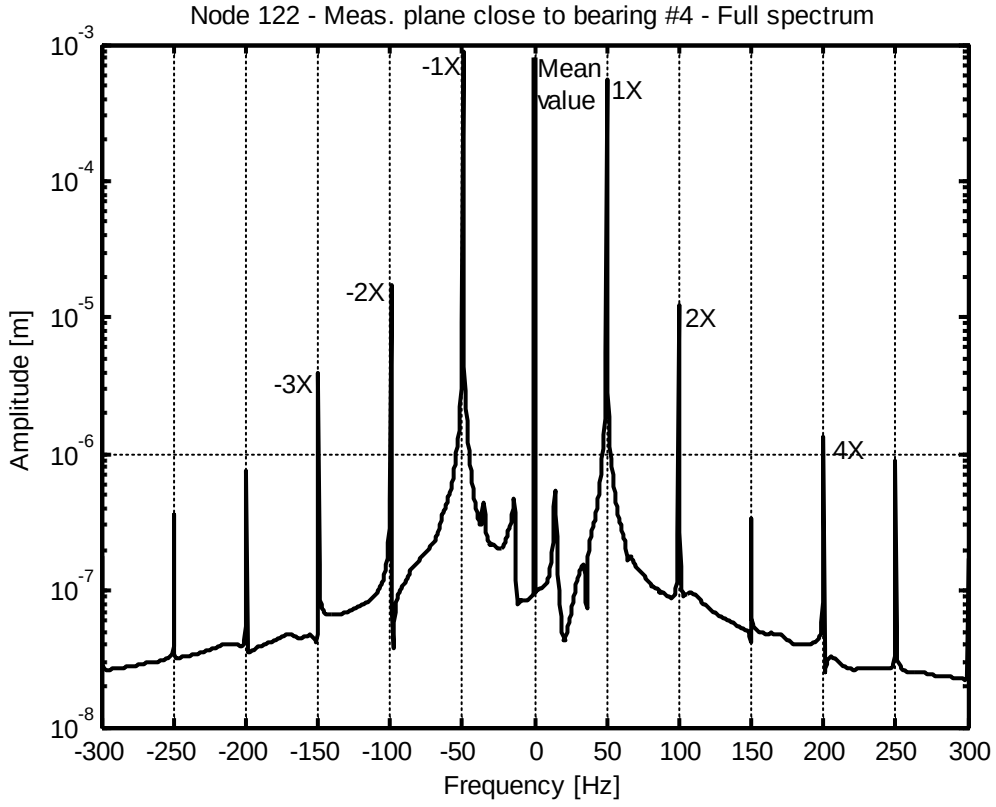

Figure 11. Full spectrum of shaft-line orbit close to bearing #4 in case of radial misalignment of 100 μm @ 90° and angular misalignment of 15 mrad @ 0°.

It is also interesting to consider the effect of the increase of the radial or of the angular misalignment, *ceteris paribus*. Figure 12 shows the orbits in the measuring plane close to bearing #1 for increasing values of radial misalignment from 50 to 200 μm. It is possible to note how the dimension of the orbits is increasing, i.e. vibration amplitudes along measuring directions are increasing. Also orbit shapes are deviating from the elliptical shape, clearly indicating the presence of superharmonic components. Similar results can be drawn by considering figure 13, which shows the orbits in the same measuring plane for increasing values of angular misalignment from 5 to 35 mrad.

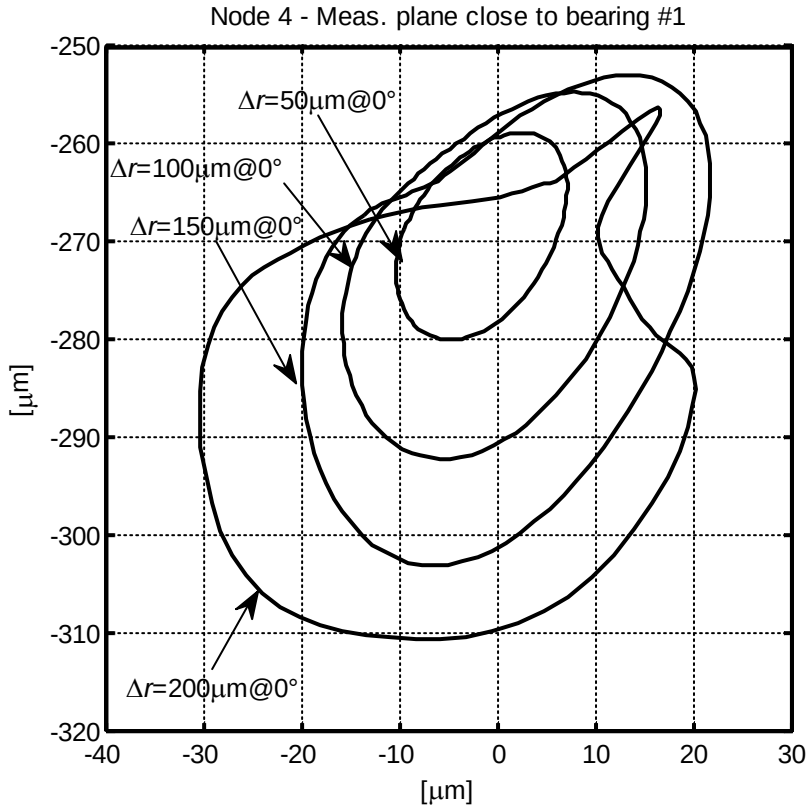

Figure 12. Comparison of orbits in the measuring plane close to bearing #1 for different radial misalignments.

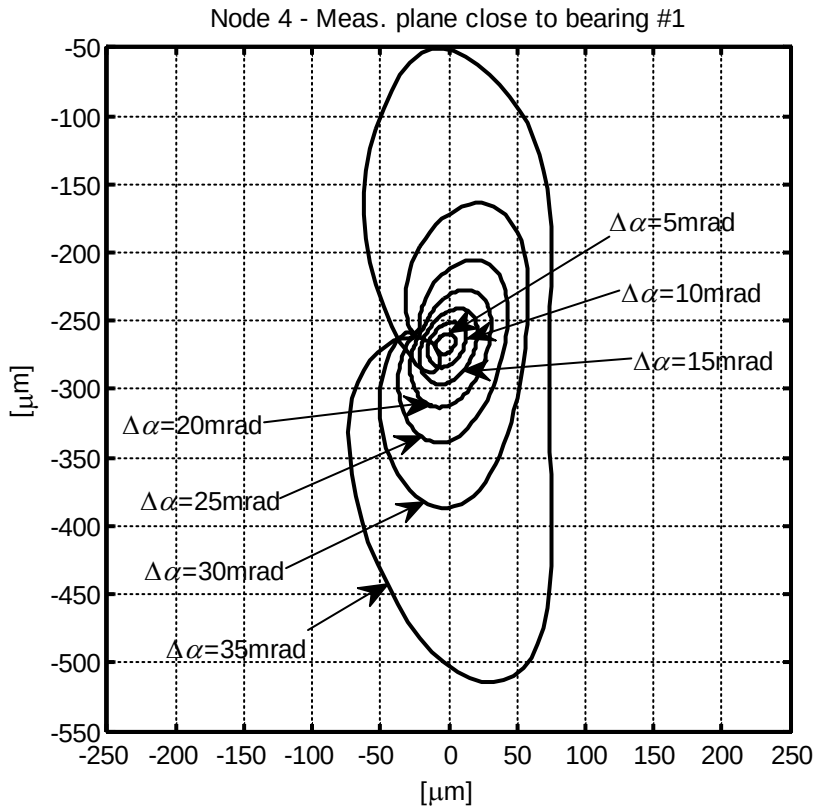

Figure 13. Comparison of the orbits in the measuring plane close to bearing #1 for different angular misalignments.

4.2. Effect of radial misalignment

As it has been shown in the previous section, the model is able to consider simultaneously both radial and angular misalignment, with arbitrary combination of amplitudes and phases, and to explain the arising of nonlinear effects. However, because of the infinite possible combinations of radial and angular misalignments, a comprehensive analysis is rather awkward. Thus, the effects of radial and angular misalignments are analysed separately, starting from the former one.

In order to evaluate the “degree” of nonlinearity, the ratios between the superharmonic component amplitudes and the synchronous one are considered. Moreover, the harmonic components along the two principal directions, vertical and horizontal, are considered, because these are the directions of the measuring probes on actual machines. In this way, it is easier to give pertinent diagnostic information.

Figure 14 and figure 15 show 2X/1X, 3X/1X and 4X/1X amplitude ratios respectively for the vertical and the horizontal directions and for the vibration measuring planes close to bearings from #1 to #4. Radial misalignment magnitudes are in the range from 50 to 210 μm with phase of 0°, i.e. in phase with the unbalance.

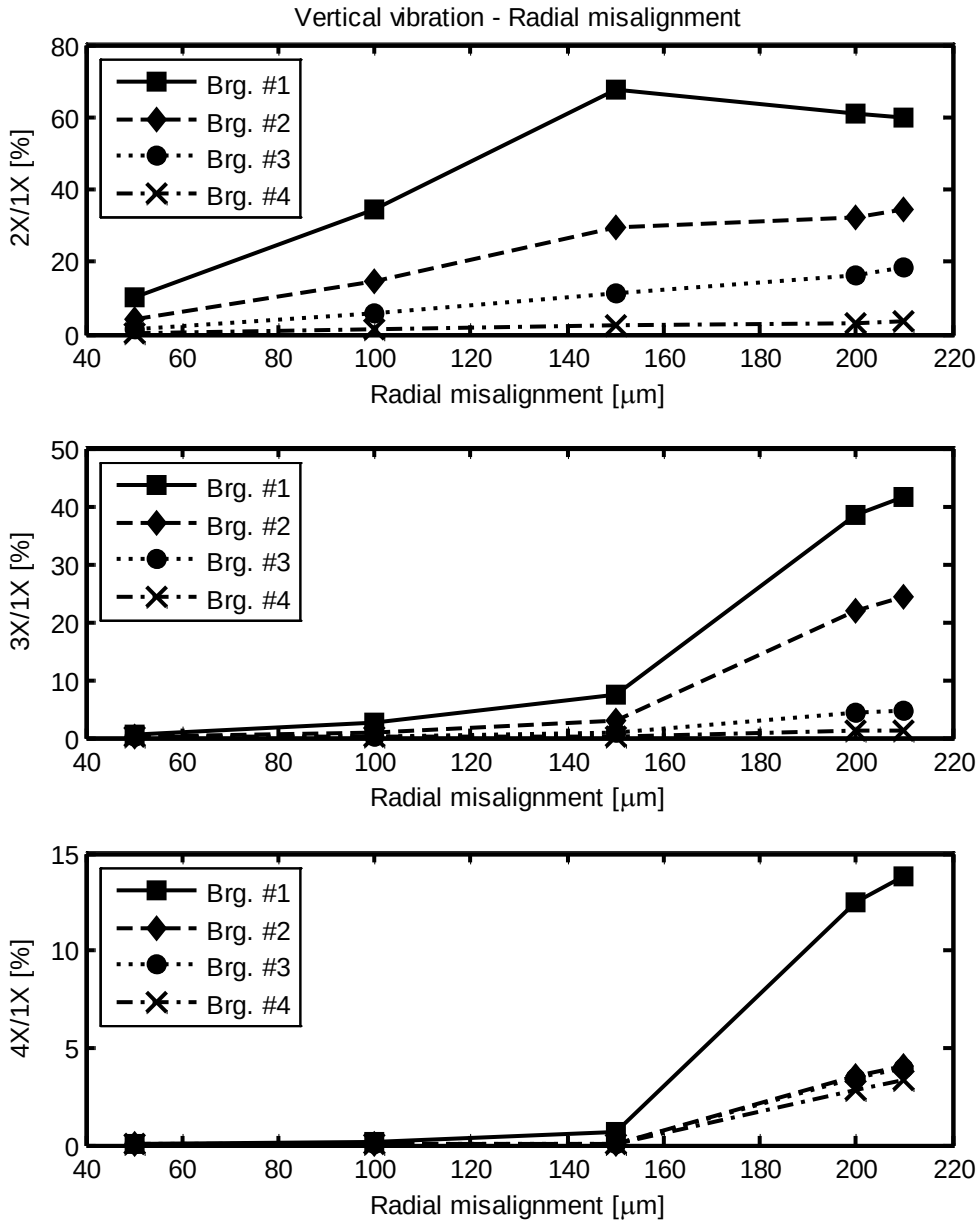

Figure 14. Vertical vibration in bearings from #1 to #4: 2X/1X, 3X/1X and 4X/1X amplitude ratios for increasing magnitudes of radial misalignment @ 0°.

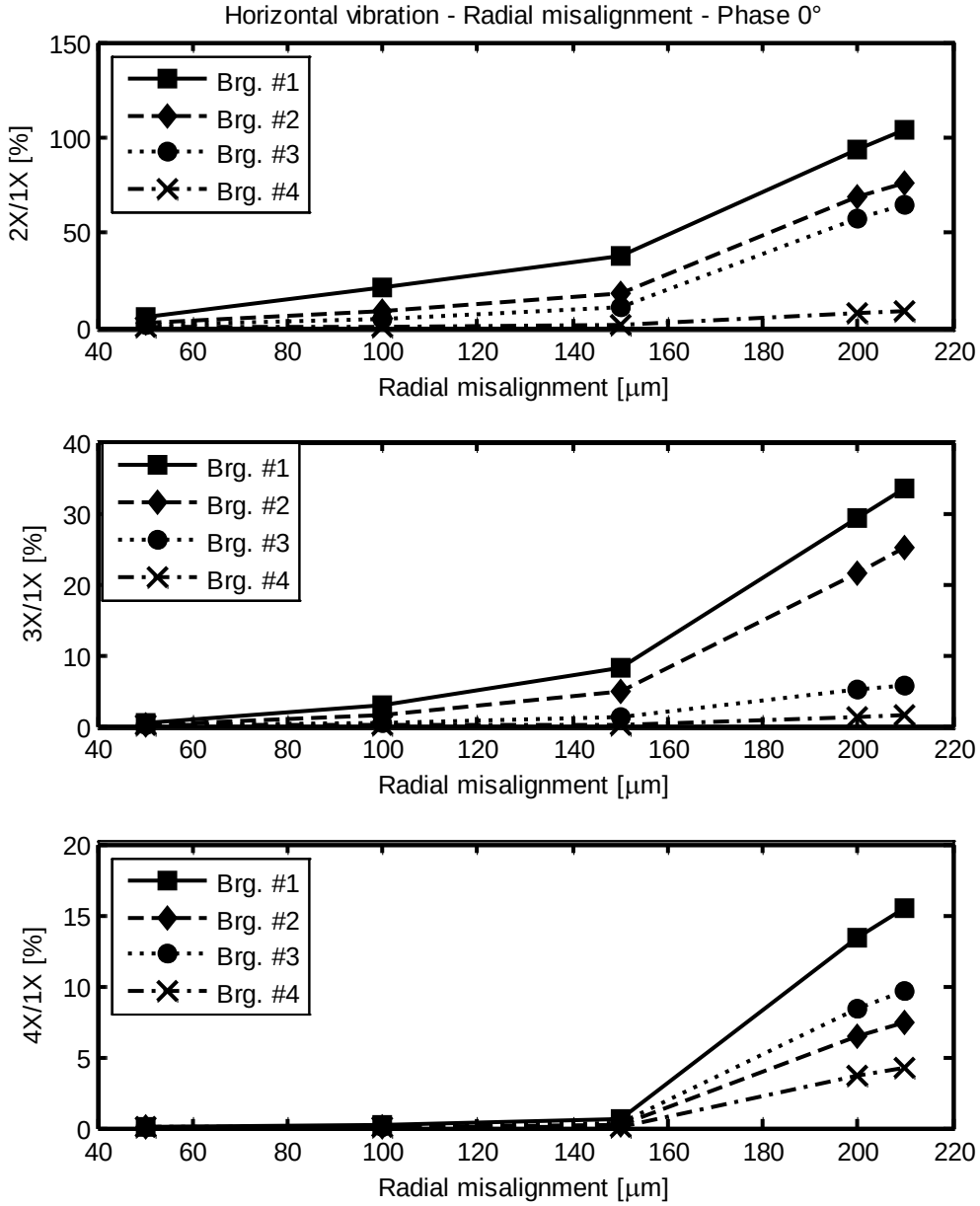

Figure 15. Horizontal vibration in bearings from #1 to #4: 2X/1X, 3X/1X and 4X/1X amplitude ratios for increasing magnitudes of radial misalignment @ 0°.

With the exception of the 2X/1X amplitude ratio for the vertical direction in bearing #1, the ratios have more than linear increasing trends as a function of radial misalignment magnitude. The contribution of 4X components becomes significant only for high radial misalignment magnitude. 2X horizontal component becomes almost equal to 1X one for bearing #1 when the misalignment is 210 μm.

For the considered machine model, if the radial misalignment is imposed in quadrature to the unbalance, the increasing of the ratios becomes quicker than in the case of 0° phase, as shown in figure 16 and figure 17 for the 2X/1X ratio and the vertical direction only. In this case, 2X amplitude is about equal to 1X amplitude in horizontal direction and about one and half in vertical direction, when the radial misalignment is 100 μm. Similar results, in terms of quick increasing when the misalignment phase is 90°, are obtained for 3X/1X and 4X/1X ratios.

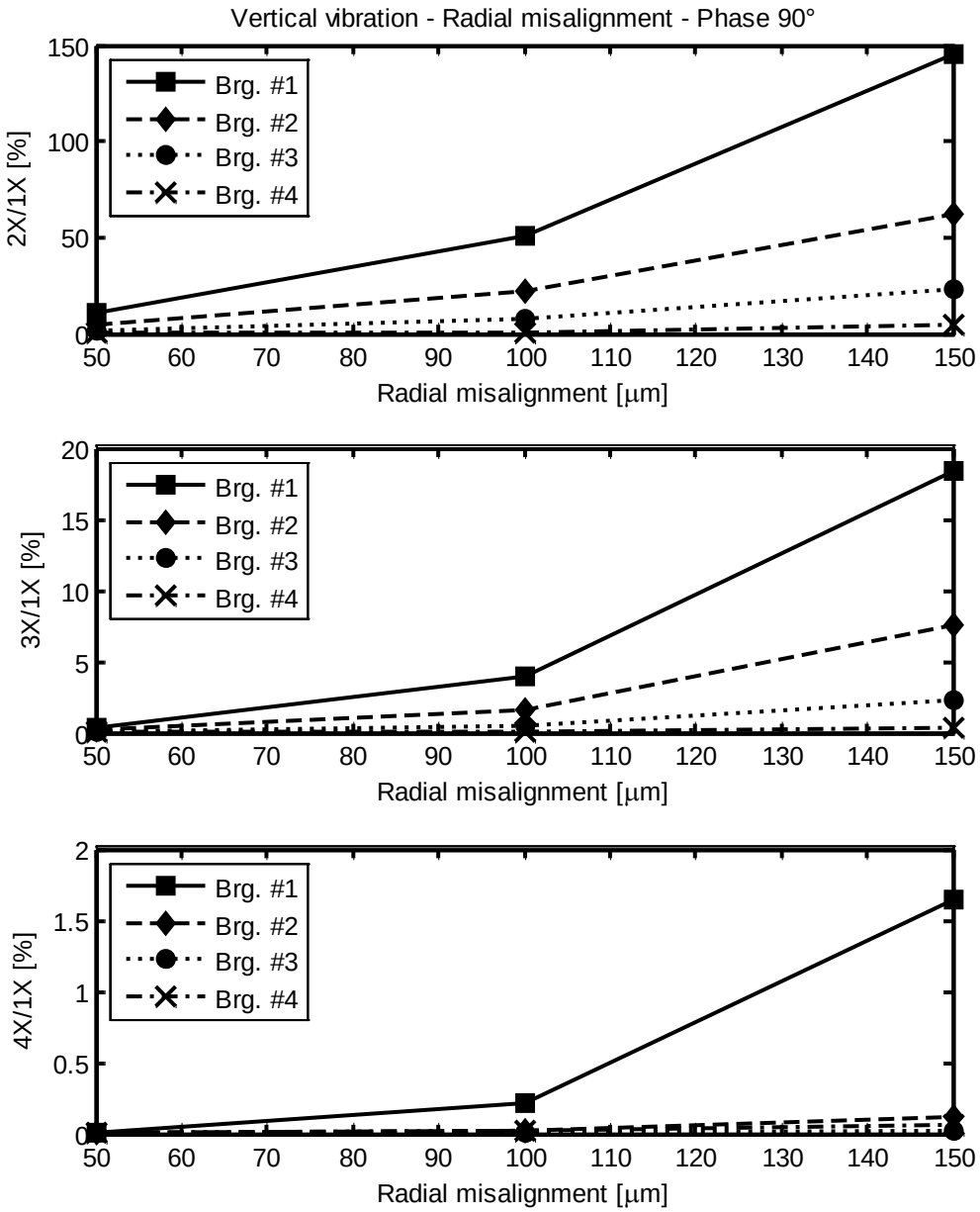

Figure 16. Vertical vibration in bearings from #1 to #4: 2X/1X, 3X/1X and 4X/1X amplitude ratios for increasing magnitudes of radial misalignment @ 90°.

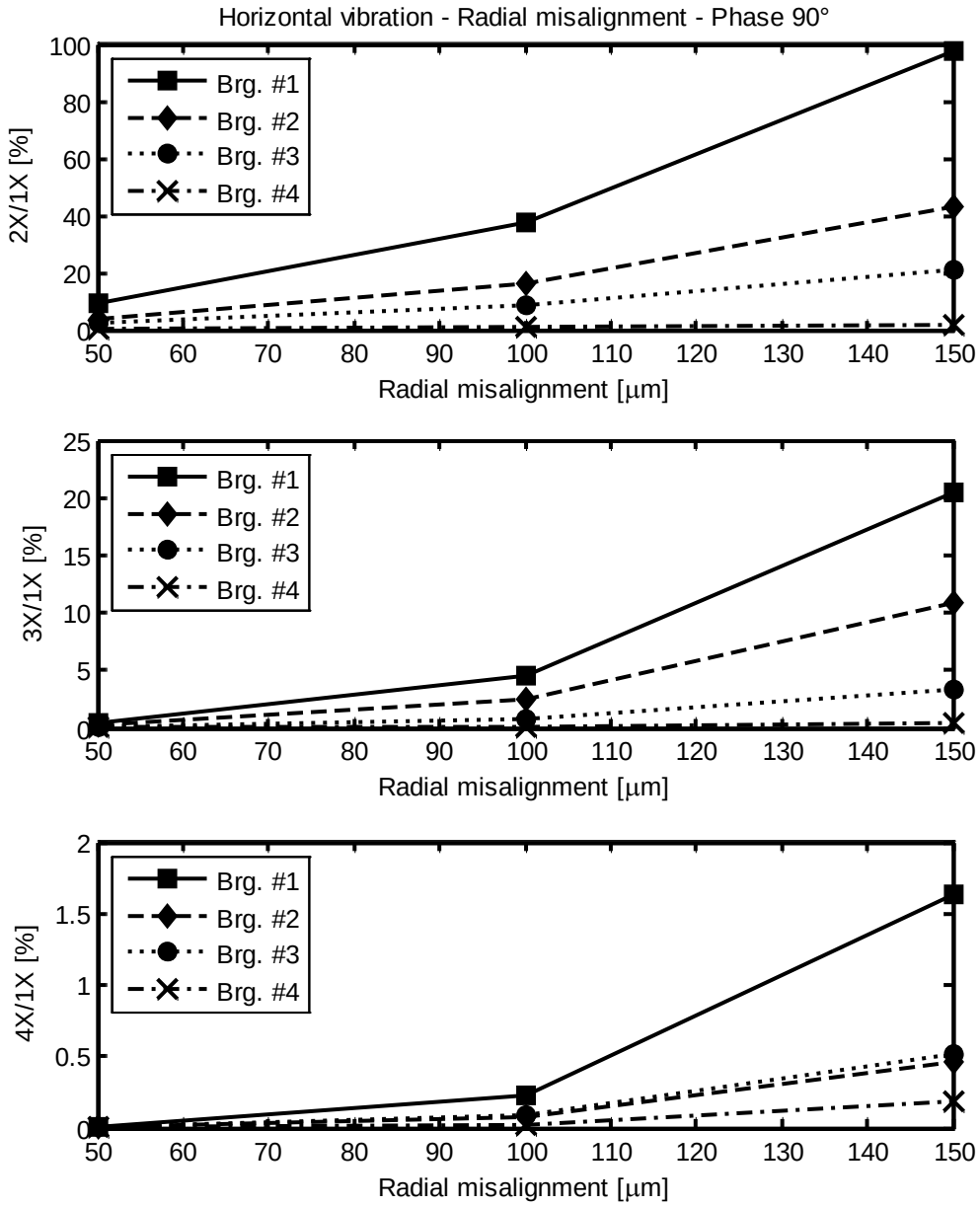

Figure 17. Horizontal vibration in bearings from #1 to #4: 2X/1X, 3X/1X and 4X/1X amplitude ratios for increasing magnitudes of radial misalignment @ 90°.

4.3. Effect of angular misalignment

The effect of increasing magnitude of angular misalignment from 5 to 35 mrad with phase of 0° is shown in figure 18 and figure 19. Also in this case, nonlinear effects are evident. Even if the direct vibrations, corresponding to the maximum value of the considered angular misalignment, are comparable to those of the maximum value of radial misalignment, the ratio between the superharmonics components and the 1X component is greater.

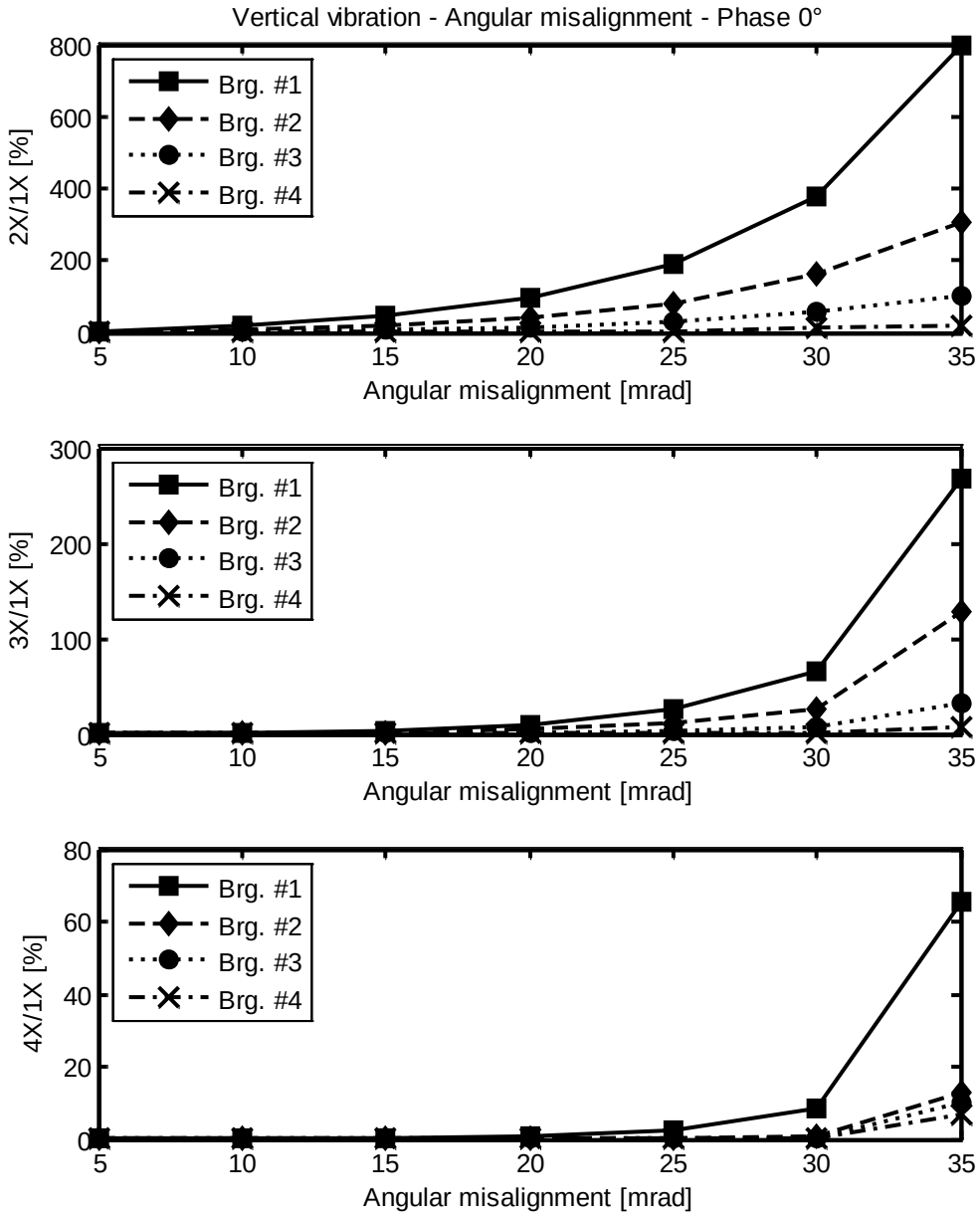

Figure 18. Vertical vibration in bearings from #1 to #4: 2X/1X, 3X/1X and 4X/1X amplitude ratios for increasing magnitudes of angular misalignment @ 0°.

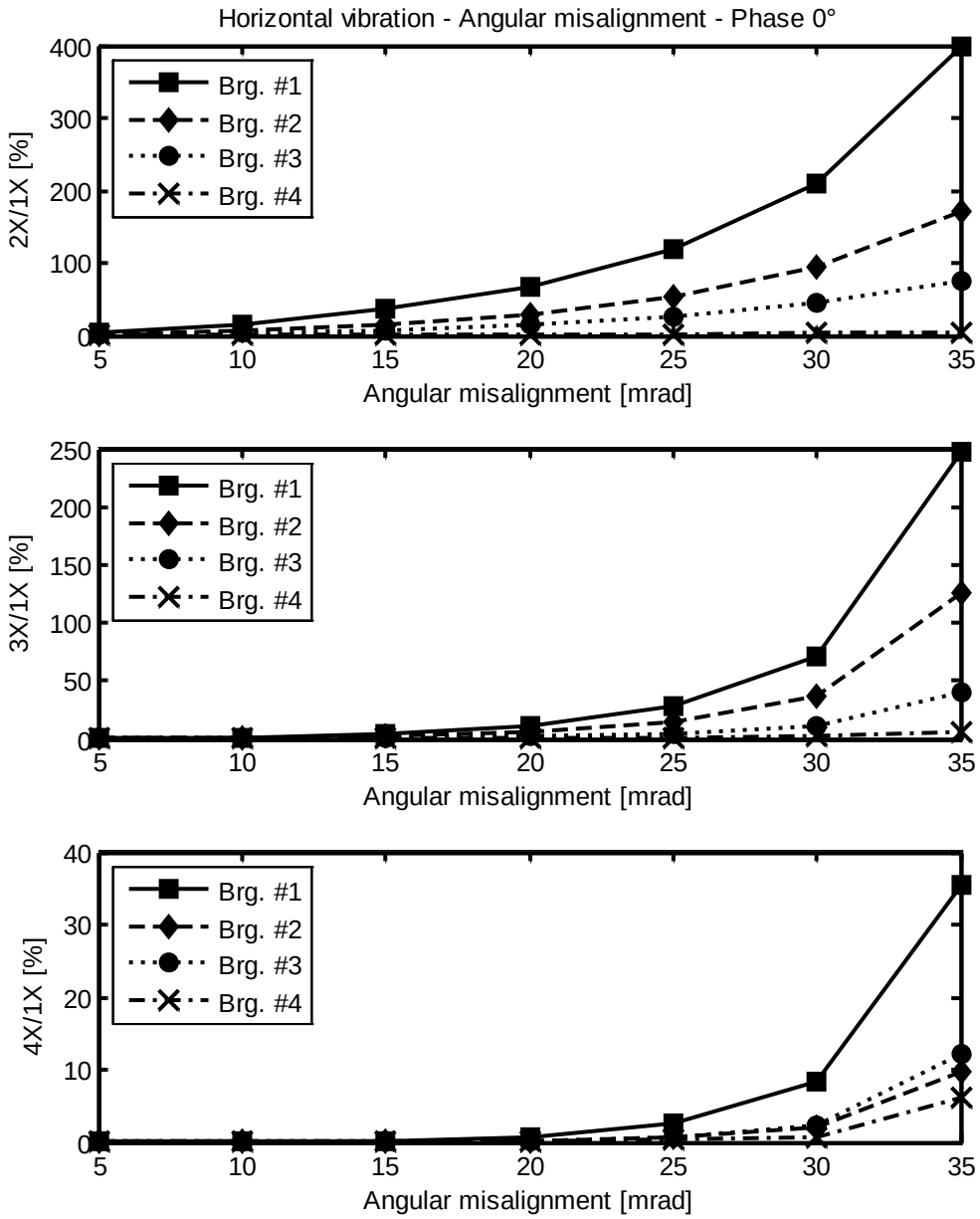

Figure 19. Horizontal vibration in bearings from #1 to #4: 2X/1X, 3X/1X and 4X/1X amplitude ratios for increasing magnitudes of angular misalignment @ 0°.

5. CONCLUSIONS

Several studies in literature deal with rotor misalignment, but it looks like that this term is used to indicate different physical processes. In the paper, the authors have dealt with rigid coupling misalignment of a hyperstatic shaft-line equipped with journal bearings. A general method, suitable for every kind of rotating machine, has been presented in detail. The model allows considering both radial and angular misalignment, separately or combined.

In order to show the effects that are caused by rigid coupling misalignment, some simulations are presented by considering a shaft-line reproducing a real turbine unit. The results of the simulations highlighted the presence of nonlinear effects in the system response: superharmonic components are the most remarkable effects of rigid coupling misalignment and are due to the variable loading on the bearings. The ratios between higher order harmonic components and

synchronous vibrations are analyzed. These results allow giving diagnostic information about the signature of this type of fault.

6. REFERENCES

1. Muszyńska A. (2005) Rotordynamics. Taylor & Francis Group - CRC Press book, New York, USA.
2. Lees A.W. (2007) Misalignment in rigidly coupled rotors. Journal of Sound and Vibration, 305 (1-2), 261-271.
3. Boyd J. (1969) Bearing misalignment—Part 1. Lubrication Eng., 25(8), 326-327.
4. Boyd J. (1969) Bearing misalignment—Part 2. Lubrication Eng., 25(9), 366.
5. Bou-Saïd B., Nicolas D. (1992) Effect of misalignment on static and dynamic characteristics of hybrid bearing, Tribology Transactions, 35(2), 325-311.
6. Prabhu B.S. (1997) An experimental investigation on the misalignment effects in journal bearings. Tribology International, 40(2), 235-242.
7. Bouyer J., Fillon M. (2002) An experimental analysis of misalignment effect on hydrodynamic plain journal bearing performances. Transactions of the ASME – Journal of Tribology, 124(2), 313-319.
8. Bently D.E. (2002) Fundamentals of Rotating Machinery Diagnostics. Bently pressurized Bearings Press, Minden, NV, USA.
9. Xu M., Marangoni R.D. (1994) Vibration analysis of a motor-flexible coupling-rotor system subject to misalignment and unbalance, Part I: Theoretical model and analysis. Journal of Sound and Vibration, 176(5), 663-679.
10. Xu M., Marangoni R.D. (1994) Vibration analysis of a motor-flexible coupling-rotor system subject to misalignment and unbalance, Part II: Experimental validation. Journal of Sound and Vibration, 176(5), 681-691.
11. Sekhar A.S., Prabhu B.S. (1995) Effects of coupling misalignment on vibrations of rotating machinery. Journal of Sound and Vibration, 185(4), 655-671.
12. Gibbons C.B (1979) Coupling Misalignment Forces. Proc. of 5th Turbomachinery Symposium, Texas A&M University, College Station, USA, 111-116.
13. Lee Y.-S., Lee C.-W. (1999) Modelling and vibration analysis of misaligned rotor-ball bearing systems. Journal of Sound and Vibration, 224(1), 17-32.
14. Hu W., Miah H., Feng N.S., Hahn E.J. (2000) A Rig for Testing Lateral Misalignment Effects in a Flexible Rotor Supported on Three or More Hydrodynamic Journal Bearings. Tribology International, 33 (3-4), 197-204.
15. Al-Hussain K.M., Redmond I. (2002) Dynamic response of two rotors connected by rigid mechanical coupling with parallel misalignment. Journal of Sound and Vibration, 249(3), 483-498.
16. Al-Hussain K.M., (2003) Dynamic stability of two rigid rotors connected by a flexible coupling with angular misalignment. Journal of Sound and Vibration, 266(2), 217-234.
17. Patel T.H., Darpe A.K. (2009) Experimental investigations on vibration response of misaligned rotors. Mechanical Systems and Signal Processing, 23(7), 2236-2252.
18. Patel T.H., Darpe A.K. (2009) Vibration response of misaligned rotors, Journal of Sound and Vibration, 325(3), 609-628.
19. Prabhakar S., Sekhar A.S., Mohanty A.R. (2001) Vibration analysis of a misaligned rotor-coupling-bearing system passing through the critical speed. IMechE Proceedings of the Institution of Mechanical Engineers Part C-Journal of Mechanical Engineering Science, 215, part C, 1417-1428.
20. Peng Z., Chu F., He Y. (2002) Vibration signal analysis and feature extraction based on reassigned wavelet scalogram. Journal of Sound and Vibration, 253(5), 1087-1100.
21. Peng Z., He Y., Chen Z., Chu F. (2002) Identification of the shaft orbit for rotating machines using wavelet modulus maxima. Mechanical Systems and Signal Processing, 16(4), 623-635.
22. Sinha J.k., Lees A.W., Friswell M.I. (2004) Estimating unbalance and misalignment of a flexible rotating machine from a single run-down. Journal of Sound and Vibration, 272, 967-989.
23. Saavedra, P.N., Ramírez, D.E. (2004) Vibration analysis of rotors for the identification of shaft misalignment – Part 1: theoretical analysis. IMechE Proceedings of the Institution of Mechanical Engineers Part C-Journal of Mechanical Engineering Science, 218(9), 971-985.
24. Saavedra, P.N., Ramírez, D.E. (2004) Vibration analysis of rotors for the identification of shaft misalignment – Part 2: experimental validation. IMechE Proceedings of the Institution of Mechanical Engineers Part C-Journal of Mechanical Engineering Science, 218(9), 987-999.

25. Bachschmid N., Pennacchi P. (2003) Accuracy of fault detection in real rotating machinery using model based diagnostic techniques. JSME International Journal Series C, 46(3), 1026-1034.
26. Pennacchi P., Vania A. (2005) Diagnosis and model based identification of a coupling misalignment. Shock and Vibration, 12(4), 293-308.
27. Tsai C.-Y., Huang S.-C. (2009) Transfer matrix for rotor coupler with parallel misalignment. Journal of Mechanical Science and Technology, 23(5), 1383-1395.
28. Bahaloo H., Ebrahimi A., Samadi M. (2009) Misalignment Modeling in Rotating Systems. Proceedings of ASME Turbo Expo 2009: Power for Land, Sea and Air, GT2009, June 8-12, 2009, Orlando, Florida, USA, paper GT2009-60121, 1-7.
29. Lalanne M., Ferraris G. (1998) Rotordynamics Predictions in Engineering. John Wiley & Sons Inc., Chichester, England.
30. Childs D.W. (1993) Turbomachinery Rotordynamics. John Wiley & Sons Inc, Chichester, England.
31. Wowk V. (2000) Machine Vibration: Alignment. Mc Graw-Hill, New York.
32. Bachschmid N., Pennacchi P., Vania A. (2002) Identification of Multiple Faults in Rotor Systems. Journal of Sound and Vibration, 254(2), 327-366.
33. Someya T. (1989) Journal-Bearing Databook. Springer-Verlag, Berlin, Germany.
34. Stachowiak G.W., Batchelor A.W. (2005) Engineering Tribology. Butterworth Heinemann, Burington, USA.
35. Pennacchi P., Bachschmid N., Vania A., Zanetta G.A., L. Gregori (2006) Use of Modal Representation for the Supporting Structure in Model Based Fault Identification of Large Rotating Machinery: Part 1 – Theoretical Remarks. Mechanical Systems and Signal Processing, 20(3), 662-681.
36. Pennacchi P., Bachschmid N., Vania A., Zanetta G.A., Gregori L. (2006) Use of Modal Representation for the Supporting Structure in Model Based Fault Identification of Large Rotating Machinery: Part 2 – Application to a Real Machine, Mechanical Systems and Signal Processing, 20(3), 682-701.

j index;

$\mathbf{x}_j^{(r)}$ generalized displacement vector of j^{th} rotor node;

$x_j^{(r)}$ vertical displacement of j^{th} rotor node;

$y_j^{(r)}$ horizontal displacement of j^{th} rotor node;

$\vartheta_{x_j}^{(r)}$ rotation about horizontal direction of j^{th} rotor node;

$\vartheta_{y_j}^{(r)}$ rotation about vertical direction of j^{th} rotor node;

n_r number of rotor nodes;

$\mathbf{x}^{(r)}$ generalized displacements of all the rotor nodes;

$[\mathbf{M}^{(r)}]$ mass matrix of the rotor;

$[\mathbf{C}^{(r)}]$ internal damping matrix of the rotor;

$[\mathbf{K}^{(r)}]$ stiffness matrix of the rotor;

$[\mathbf{G}^{(r)}]$ gyroscopic matrix;

n_b number of the journal bearings;

I_c set of the indexes of the rotor nodes corresponding to a journal bearing;

$\mathbf{x}_c^{(r)}$ vector of the generalized displacement of the constrained nodes;

$\mathbf{x}_f^{(r)}$ vector of the generalized displacement of the free nodes;

n_C number of rotor couplings;

$\Delta\alpha$ magnitude of the angular misalignment;

φ_α phase of the angular misalignment with respect to rotor phase reference;

Δr magnitude of the radial misalignment;

φ_r phase of the angular misalignment with respect to rotor phase reference;

j_C index of the coupling node;

Ω rotational speed;

i imaginary unit;

e Euler's number;

$\Delta\mathbf{x}_j$ generalized displacements imposed the shaft by coupling misalignment, on the d.o.f.s corresponding to the j_C^{th} coupling node;

θ angular position of the rotor;

$\Delta\mathbf{x}$ generalized displacements imposed the shaft by coupling misalignment;

Subscripts:

$_j$ index;

$_c$ constrained;

$_f$ free;

$_\alpha$ angular misalignment;

$_r$ radial misalignment;

$_C$ coupling;

Superscripts:
$^{(r)}$ rotor;